

# Enhanced passive thermal stealth properties of VO<sub>2</sub> thin films via gradient W doping

**Hyuk Jin Kim,<sup>a,†</sup> Young Hwan Choi,<sup>a,†</sup> Dongkyu Lee,<sup>a,b</sup> In Hak Lee,<sup>a,c</sup> Byoung Ki Choi,<sup>a</sup>  
Soo-Hyon Phark,<sup>d,e</sup> and Young Jun Chang<sup>a,b,\*</sup>**

*<sup>a</sup>Department of Physics, University of Seoul, Seoul 02504, Korea,*

*<sup>b</sup>Department of Smart Cities, University of Seoul, Seoul 02504, Korea,*

*<sup>c</sup>Center for Spintronics, Korea Institute of Science and Technology, Seoul 02792, Korea,*

*<sup>d</sup>Center for Quantum Nanoscience, Institute for Basic Science, Seoul 03760, Korea,*

*<sup>e</sup>Department of Physics, Ewha Womans University, Seoul 03760, Korea.*

## ABSTRACT

Thermal stealth and camouflage have been intensively studied for blending objects with their surroundings against remote thermal image detection. Adaptive control of infrared emissivity has been explored extensively as a promising way of thermal stealth, but it still requires an additional feedback control. Passive modulation of emissivity, however, has been remained as a great challenge which requires a precise engineering of emissivity over wide temperature range. Here, we report a drastic improvement of passive camouflage thin films capable of concealing thermal objects at near room temperature without any feedback control, which consists of a vanadium dioxide (VO<sub>2</sub>) layer with gradient tungsten (W) concentration. The gradient W-doping widens the metal-insulator transition width, accomplishing self-adaptive thermal stealth with a smooth change of emissivity. Our simple approach, applicable to other similar thermal camouflage materials for improving their passive cloaking, will find wide applications, such as passive thermal camouflage, urban energy-saving smart windows, and improved infrared sensors.

**Keywords:** Vanadium dioxide (VO<sub>2</sub>), Thermal stealth, Infrared emission, Metal-insulator transition (MIT), Transmission electron microscopy (TEM)

\*Corresponding author.: \* yjchang@uos.ac.kr (Y.J. Chang)

† These authors have contributed equally to this work.

## I. INTRODUCTION

Thermal stealth and camouflage concern the hiding of objects, such as military artillery and soldiers, from remote thermal detection devices like infrared (IR) cameras[1–4]. Thermal radiation is proportional to not only surface temperature of an object, but also its thermal radiation emissivity ( $\epsilon$ ) for a given radiation wavelength. The IR cameras sense thermal radiation in the wavelength range 7.5 to 14  $\mu\text{m}$ , and are capable of detecting objects with elevated surface temperatures in the dark[3]. However, if  $\epsilon$  of the object surface is artificially manipulated, the IR detection cannot distinguish a hot object with reduced  $\epsilon$  value. Therefore, an ability to control  $\epsilon$  would be beneficial for thermal stealth applications.

Electrochromic materials[5–7], optical nanostructures[8,9], plasmonic resonators[10,11], and metal-insulator transition (MIT) materials[12–15], have been reported to enable control of thermal emissivity. In particular,  $\text{VO}_2$ [12,13],  $(\text{La,Sr})\text{MnO}_3$ [16] and rare earth nickelate[15], have been recently suggested to be MIT materials promising for thermochromic switching and urban energy-saving smart window applications[17–19]. MIT is the result of band gap opening at the MIT temperature ( $T_{\text{MIT}}$ ), which results in huge changes of  $\epsilon$  in IR region (for example, metallic silver ( $\epsilon = 0.02$ ) and dielectric glass (0.95)) and corresponding changes in surface temperatures measured by IR sensor ( $T_{\text{IR}}$ ). Thermal stealth application requires a wide range of active temperature ( $>30^\circ\text{C}$ ) at near the room temperature, however the reported MIT materials have been limited in applications due to their narrow  $T_{\text{MIT}}$  window (usually,  $<10^\circ\text{C}$ )[12–15]. To extend the temperature window, active control systems, such as a joule heater, are required[2].

Vanadium dioxide ( $\text{VO}_2$ ) is one of the most widely studied MIT materials[12]. In the bulk phase,  $\text{VO}_2$  undergoes a very sharp MIT at  $68^\circ\text{C}$  with MIT width ( $W_{\text{MIT}}$ ) of  $<1^\circ\text{C}$  and a band gap opening of  $\sim 0.5$  eV. This results in large reversible changes in its IR absorption coefficient and

electrical resistance[20], and it is the reason why VO<sub>2</sub> films are being considered for thermochromic, thermal stealth[13], smart window[17], and IR-sensing bolometer applications[21]. VO<sub>2</sub> thin films exhibit MIT-induced electrical resistivity changes of 2–4 orders of magnitude and W<sub>MIT</sub> of 5-10°C[22,23]. Variety of oxidation phases (V<sub>2</sub>O<sub>3</sub>, V<sub>2</sub>O<sub>5</sub>, V<sub>6</sub>O<sub>13</sub>, and so on) are found to coexist with VO<sub>2</sub>, and the MIT properties of VO<sub>2</sub> show a considerable dependence on the strain and stoichiometry. Meanwhile there have been studies on VO<sub>2</sub> thin films doped with tungsten[24–27] or molybdenum[28] to tune their MIT characteristics. Despite enormous efforts to understand the VO<sub>2</sub> thin films by means of various growth techniques such as using sol-gel[29], chemical vapor deposition[30], pulsed laser deposition[31,32], molecular beam epitaxy[23], atomic layer deposition[33] and reactive sputtering[34,35], however, a straightforward method of synthesizing VO<sub>2</sub> thin films with predetermined T<sub>MIT</sub> and W<sub>MIT</sub> values are remained as a challenging task.

In this work, we studied the near-room temperature IR emission properties of W-doped VO<sub>2</sub> (W-VO<sub>2</sub>) films prepared on SiO<sub>2</sub>, quartz, or mica substrates by vacuum evaporation and subsequent thermal oxidation. In contrast to a narrow emissivity transition temperature window, i.e. W<sub>MIT</sub> ~5°C, observed in the pure VO<sub>2</sub> films, the W-VO<sub>2</sub> films showed much enhanced W<sub>MIT</sub> up to 45°C, which is large enough for practical thermal stealth application. A cross-sectional transmission electron microscopy (TEM) examination of the W-VO<sub>2</sub> films revealed that the W concentration is gradually distributed with the distance from the film-substrate interface within W-VO<sub>2</sub> layer. We discuss the implications of this observation in terms of the increased W<sub>MIT</sub> in the W-VO<sub>2</sub> films and the large deviation of the T<sub>MIT</sub> behavior from that in the pure VO<sub>2</sub> films as well.

## II. EXPERIMENTAL

We prepared VO<sub>2</sub> and W-VO<sub>2</sub> films on SiO<sub>2</sub>/Si, quartz, and mica substrates in two steps. Initially, V or WO<sub>3</sub> layers were deposited by electron-beam evaporation at room temperature at a deposition rate of 0.6 Å/s in a high-vacuum chamber (base pressure of 5×10<sup>-8</sup> torr). For VO<sub>2</sub> films, we controlled the thickness of the V layer ( $t_v$ ) from 20 to 100 nm and investigated the effect of VO<sub>2</sub> film thickness on IR emission. To form W-VO<sub>2</sub> films, a stack of alternating V and WO<sub>3</sub> layers (V-W) of 96 nm thick in total were deposited ( $t_{v-w}$ ) by three V (30 nm) and WO<sub>3</sub> (2 nm) deposition cycles, which resulted in a tungsten to vanadium ratio of 0.03:1. Both the deposited V and V-W layers were then annealed in the tube vacuum furnace at 400-430°C for 4-5 h (for VO<sub>2</sub>) or 480-500°C for 1 h (for W-VO<sub>2</sub>), respectively. During the annealing, an oxygen partial pressure (PO<sub>2</sub>) of 0.2 torr was maintained with 99.999% O<sub>2</sub> gas flow (45 sccm) while pumping the tube furnace with a rotary vacuum pump [35]. The PO<sub>2</sub> was chosen after comparing the MIT behavior of VO<sub>2</sub> films treated at several different conditions.

Crystallinities of samples were checked by high-resolution x-ray diffraction (HRXRD, Smartlab 9kW, Rigaku) and by cross-sectional TEM imaging with chemical analysis (JEM-ARM200F, JEOL). For TEM, we used a Schottky-type field-emission gun (FEG) operated at 200 keV and prepared cross-sectional specimens by conventional cutting, gluing, polishing, and ion milling (PIPS 691, GATAN) at 5 keV. To study the MIT behaviors of the films, we measured four-probe electrical resistances in the temperature range of 20-100°C by using a closed-cycle refrigerator equipped with a nanovoltmeter (Keithley 2182A), a programmable current source (Keithley 224), and a temperature controller (Lakeshore 330) under a vacuum condition (<1×10<sup>-4</sup> torr). An IR camera (FLK-Ti400 (detector resolution 320×240 pixels), FLUKE) was used to measure T<sub>IR</sub> values of films and bare substrates, while specimens were uniformly heated on a Shamal hot plate (HHP-411, Iuchi Seiei Dou). T<sub>IR</sub> values of films were

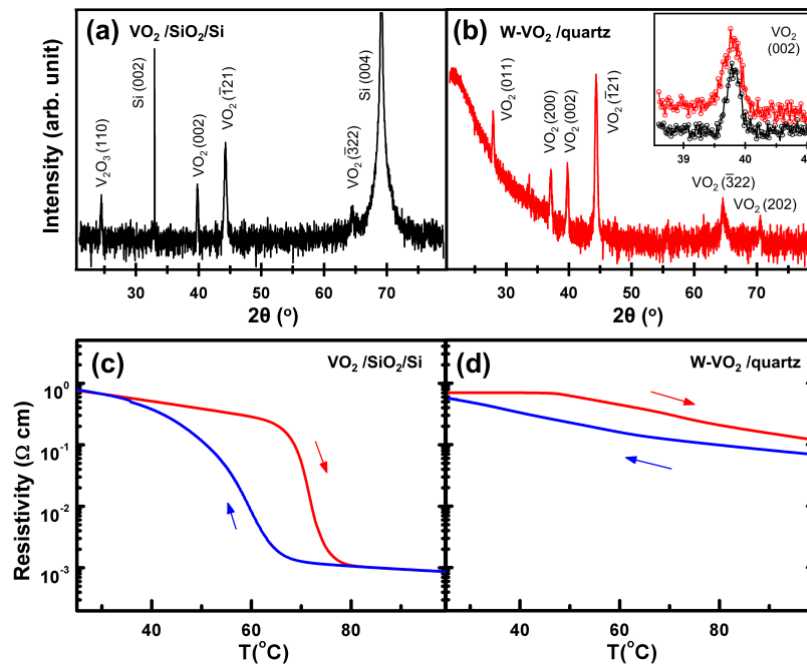
determined by comparing them with the temperature of substrates ( $T_s$ ), where  $T_{IR}$  values of the hot plate were calibrated with a thermocouple sensor attached to the hot plate for each time. Also, the emissivity was measured by changing the emissivity of the thin films in the IR camera until  $T_{IR}$  values of films equals to the hot plate temperature [2].

### III. RESULTS AND DISCUSSIONS

Figs. 1(a) and (b) show HRXRD data of a  $VO_2$  film on  $SiO_2/Si$  and a  $W-VO_2$  film on quartz respectively. For both films, various peaks corresponding to different crystalline orientations indicate their polycrystalline character with monoclinic  $VO_2$  phase, except negligible fraction of  $V_2O_3$  phase. As shown in the inset of Fig. 1(b), the  $W-VO_2$  film shows slight shifts and broadening of (002) peaks. Compared to the undoped  $VO_2$  film, the  $W-VO_2$  film has 0.05% elongation of c-axis. According to the previous studies of thin films, 4 % W-doping is required to induce 0.8% elongation of c-axis and to lower the  $T_{MIT}$  by 120 K [25]. The relatively small change of c-axis in our  $W-VO_2$  film is probably due to both small doping concentration and possible doping gradient, which also influences broadening of the (002) peak. Figs. 1(c) and (d) show their electrical resistivity curves for increasing (red) and decreasing (blue) temperature sweeps. For the  $VO_2$  thin film, the dramatic resistivity changes with large hysteresis indicate the characteristic 1<sup>st</sup> order MIT behavior. From the sharp MIT temperatures at 71.4°C and 56.0°C during heating and cooling, the hysteresis width,  $\Delta T_{MIT} = T_{MIT}(\text{heating}) - T_{MIT}(\text{cooling})$ , is calculated to be 15.4°C. Note that  $T_{MIT}$  was determined as the temperature corresponding to the inflection point of the resistivity switching curve. The resistivity change of nearly three orders of magnitude observed in the  $VO_2$  films was comparable to those reported for both polycrystalline and epitaxial  $VO_2$  thin films[22]. On the other hand, the  $W-VO_2$  film shows small resistivity change with nearly one order of magnitude, strongly suppressed than that of the  $VO_2$  film. According to previous studies of uniformly W-doped  $VO_2$  films, W doping

gradually reduces the magnitude of resistivity change and also lowers  $T_{MIT}$ [25,26]. However, the uniformly W-doped ones could not account the small resistivity change in our W-VO<sub>2</sub> film. This discrepancy may suggest that the W-VO<sub>2</sub> film may have gradual W distribution along the out-of-plane direction, which we will discuss later.

Figure 1. Crystallinity and electrical properties of VO<sub>2</sub> and W-VO<sub>2</sub> films. HRXRD patterns of (a) VO<sub>2</sub> ( $t_v=70$  nm) film on SiO<sub>2</sub>/Si and (b) W-VO<sub>2</sub> ( $t_{v-w}=96$  nm) film on quartz. Temperature-dependent resistivity of (c) the VO<sub>2</sub> and (d) W-VO<sub>2</sub> thin films. (Inset of (b) shows comparison of VO<sub>2</sub> (002) peaks between VO<sub>2</sub> (black) and W-VO<sub>2</sub> (red) films.)



To check the thermal stealth characteristics of the VO<sub>2</sub> and W-VO<sub>2</sub> films, we captured IR images of the films and substrates on a hot plate (Fig. 2) for an increasing  $T_s$  from 35 to 90°C. At a given  $T_s$ , contrast of the images provided measures of sample  $T_{IR}$  values. Figs. 2(a-d) show the IR images of the samples taken at  $T_s$  values of (a) 35°C, (b) 60°C, (c) 75°C, and (d) 90°C. At  $T_s$  values of 35°C and 60°C (below the  $T_{MIT}=71$ °C, chosen at the midpoint of the

slope for an increasing  $T_S$  sweep) of  $VO_2$  films, the  $T_{IR}$  values of the film were almost the same as that of the  $SiO_2/Si$  substrate (white arrows in Figs. 2(a) and (b)). At  $T_S$  values above the  $T_{MIT}$ , the  $T_{IR}$  values of the films were lower than that of the  $SiO_2/Si$  substrate (black arrows in Figs. 2(c) and (d)). On the other hand, the W- $VO_2$  film showed a nearly fixed  $T_{IR}$  value (sky blue to green color scales, black stars in Fig. 2) regardless of  $T_S$  values (35–90°C), with a much wider  $T_S$  range than that of  $VO_2$  film. Such constant  $T_{IR}$  behavior weakens the IR detection of an object, which deserves an improved thermal stealth function. Although previous studies of W doping showed reduced  $T_{MIT}$  in  $VO_2$  film[25–27], such constant  $T_{IR}$  behavior has not been reported for doped  $VO_2$  films as far as our best efforts. In addition, all the films exhibit lateral uniformity in color contrast at each temperature, which is related to the lateral homogeneity of film constituents. We note that the color deviation at the perimeters or corners (' $\alpha$ ' in Fig. 2(d)) of the samples is because the region is not covered with the films due to clamps during the film growth. Small suppressions in  $T_{IR}$  values of the substrates from that of the hot plate (Fig. 2(a): 1.6°C for  $SiO_2$  and 1.5°C on quartz) were predominantly due to thermal contact and/or thermal gradient across the substrates.

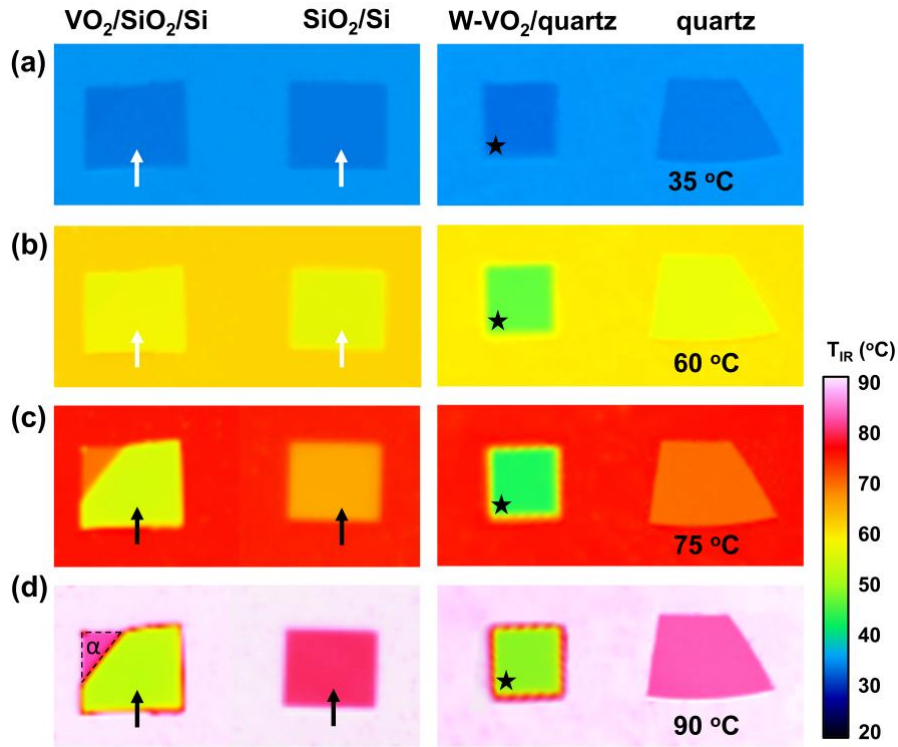


Figure 2. Thermal stealth behavior at different temperatures. (a-d) IR images of the VO<sub>2</sub> (left,  $t_v=70$  nm) and the W-VO<sub>2</sub> film (right,  $t_{v-w}=96$  nm) along with their uncoated substrates (SiO<sub>2</sub>/Si and quartz). The IR images captured at different substrate temperatures ( $T_s$ ); (a) 35, (b) 60, (c) 75, and (d) 90°C.

To obtain quantitative insight of the IR transition behaviors of the VO<sub>2</sub> and W-VO<sub>2</sub> films, we examined  $T_{IR}$  values during heating and cooling sweeps over the  $T_s$  range from 25 to 95°C (Fig. 3). VO<sub>2</sub>/SiO<sub>2</sub>/Si films showed abrupt  $T_{IR}$  transitions at  $T_{MIT}$  of 70°C (heating) and 55°C (cooling), which give a  $\Delta T_{MIT} = 15^\circ\text{C}$  (Fig. 3(a)) for different film thicknesses. Furthermore, the temperature difference between  $T_s$  and  $T_{IR}$  ( $\Delta T_{IR} = T_s - T_{IR}$ ) was monotonically enhanced on increasing  $t_v$ , which lead to a  $\Delta T_{IR}$  of  $\sim 35^\circ\text{C}$  for a VO<sub>2</sub> film of  $t_v = 100$  nm at  $T_s = 80^\circ\text{C}$  (inset of Fig. 3(a)). This observation implies that the increased thickness largely strengthens the magnitude of  $\Delta T_{IR}$ , while change of  $T_{MIT}$  is limited within  $\sim 5^\circ\text{C}$ .

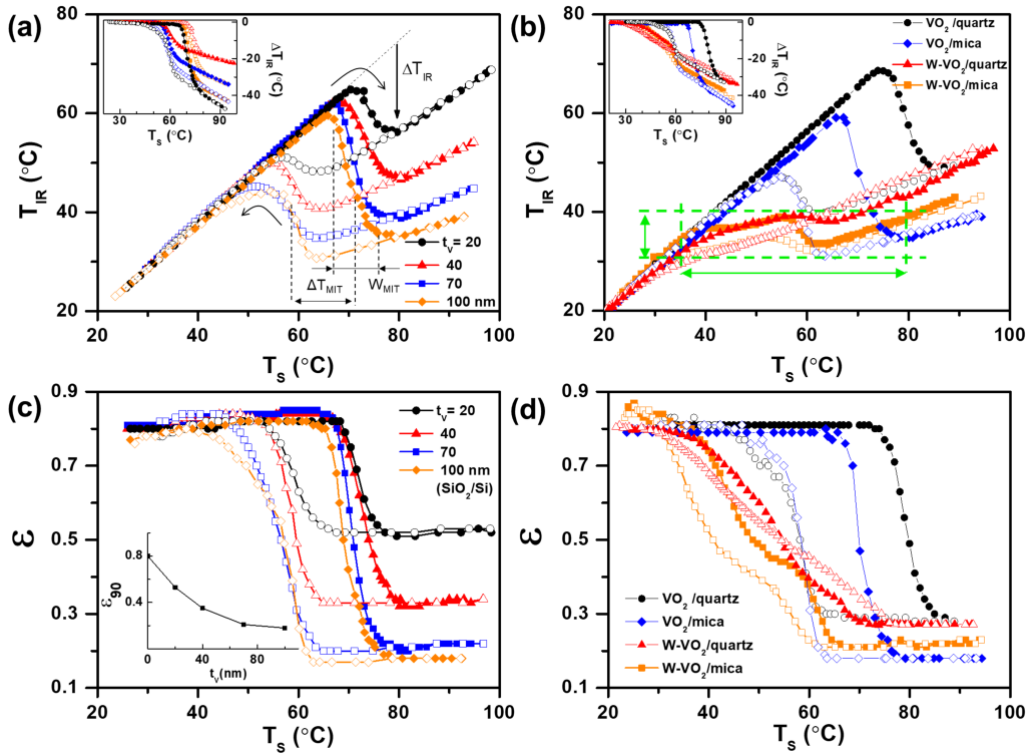


Figure 3. Quantitative analysis of IR detection. Temperature values measured by IR camera ( $T_{IR}$ ) as a function of substrate temperature ( $T_S$ ) for (a) VO<sub>2</sub> films grown on SiO<sub>2</sub>/Si substrates with different thickness ( $t_v = 20, 40, 70$  and  $100$  nm) and for (b) VO<sub>2</sub> and W-VO<sub>2</sub> films ( $t_{v-w} = 96$  nm) grown on quartz and mica substrates. Filled and empty symbols indicate heating and cooling processes, respectively. Insets in (a) and (b) are difference between  $T_S$  and  $T_{IR}$  of each thin film. Emissivity values for (c) VO<sub>2</sub> films on SiO<sub>2</sub>/Si substrates and for (d) VO<sub>2</sub> and W-VO<sub>2</sub> films on quartz and mica substrates, extracted from the  $T_{IR}$  data in (a) and (b), respectively. Inset in (c) shows thickness dependence of emissivity.

Fig. 3(b) shows  $T_{IR}$  versus  $T_S$  curves of VO<sub>2</sub> ( $t_v = 100$  nm) and W-VO<sub>2</sub> films ( $t_{v-w} = 96$  nm) prepared on quartz and mica. Similar to the films on SiO<sub>2</sub>/Si, the VO<sub>2</sub> films showed sharp  $T_{IR}$  transitions with  $\Delta T_{MIT}$  of 15–25°C, which were barely observed for the W-VO<sub>2</sub> films; the  $T_{IR}$  values remained in the range 31 to 40°C (a vertical green arrow) over a wide  $T_S$  range of 43°C

(a horizontal green arrow). In addition, the broadening of the  $T_{\text{MIT}}$ , led to the collapse of hysteresis; as shown by linear changes in  $\Delta T_{\text{IR}}$  curves in the inset of Fig. 3(b). It is worth noting that the  $\Delta T_{\text{IR}}$  values of W-VO<sub>2</sub> films became similar to those of VO<sub>2</sub> films at  $T_{\text{S}} \sim 80^\circ\text{C}$ , indicative of thermal screening effects similar to that of a VO<sub>2</sub> film at a  $T_{\text{S}}$  above the  $T_{\text{MIT}}$ . Hence, the W-doping was found to dramatically improve the thermal stealth effect of W-VO<sub>2</sub> films by transforming the sharp MIT in the VO<sub>2</sub> thin film into the gradual one for a wide temperature range.

Emissivity ( $\varepsilon$ ) of a IR spectrum band can be related a  $T_{\text{IR}}-T_{\text{S}}$  curve via thermal radiance[36], as expressed by:  $M(\lambda, T_A) = M_B(\lambda, T_A) \varepsilon(\lambda, T_A) = \frac{2\pi hc^2}{\lambda^5} \frac{1}{e^{hc/\lambda k T_A} - 1} \varepsilon(\lambda, T_A)$ , where  $M$  and  $M_B$  are the thermal radiances of material and blackbody,  $\lambda$  is wavelength,  $h$  is Planck's constant,  $c$  is speed of light,  $k$  is Boltzmann's constant, and  $T_A$  is the absolute temperature.  $T_{\text{S}}$ -dependent emissivity  $\varepsilon(T_{\text{S}})$ , shown in Figs. 3(c) and (d), is extracted from the  $T_{\text{IR}}$  versus  $T_{\text{S}}$  curves in Fig. 3(a) and (b), respectively.  $\varepsilon(T_{\text{S}})$  curves of VO<sub>2</sub> films at a given  $t_{\text{V}}$  show two saturated values, indicative of two electronic states below and above the MIT. Above the MIT, the  $t_{\text{V}}$  dependence of  $\varepsilon$  at  $T_{\text{S}} = 90^\circ\text{C}$  ( $\varepsilon_{90}$ ), shows a saturation behavior approaching  $\sim 0.2$ , indicating an optimal VO<sub>2</sub> film thickness ( $t_{\text{V}}$ ) of 100 nm. In Fig. 3(d), we show the  $\varepsilon(T_{\text{S}})$  values of W-VO<sub>2</sub> films together with VO<sub>2</sub> films, grown on quartz and mica. Here, the  $\varepsilon(T_{\text{S}})$  also saturates at 0.2-0.3, which is similar to that observed for VO<sub>2</sub> films above the  $T_{\text{MIT}}$ . However, during MIT in W-VO<sub>2</sub> films, the  $\varepsilon(T_{\text{S}})$  curves show a slow decrease over the  $T_{\text{S}}$  range of 30-70°C, which explains the monotonic behavior of the  $\Delta T_{\text{IR}}$  curves in the inset of Fig. 3(b). Furthermore, we note that substrate type has little effect on the features of  $\varepsilon(T_{\text{S}})$  curves.

Fig. 4 shows the microscopic chemical analysis to examine the correlation between the chemical compositions of W-VO<sub>2</sub> films and their  $T_{\text{IR}}$  curves (Fig. 3(b)). Fig. 4(a) shows a cross-

sectional TEM image of a W-VO<sub>2</sub> film on quartz ( $t_{V-W} = 96$  nm) and its chemical composition profile (Fig. 4(b)). The average film thickness was about 205 nm, which was in-line with thickness estimated from the volume of the VO<sub>2</sub> formed from the metallic V film as previously described[37,38]. The chemical composition mappings show laterally uniform distribution of V and W along the in-plane direction. Fig. 4(c) shows averaged concentration profiles for V, W, O, and Si along the dashed arrow shown in Fig. 4(b). Interestingly, W was densely confined towards the film surface while V was distributed rather evenly throughout the whole film thickness. These results clearly show that the doped W were distributed with concentration gradient, where the gradually modulated ratio between W and V is also shown in the inset of Fig. 4(c). Since we initially prepared the alternating layers of V and WO<sub>3</sub> at room temperature, the followed thermal oxidation process should play a critical role to form such inhomogeneous concentration distribution. According to the microscopic diffusion model, it should be noted that the oxygen anion diffusion from the surface may promotes a diffusion of cation (probably V) toward the surface to maintain the charge neutrality during the thermal oxidation[39–41]. In the meantime, the oxidation of diffused V forms granular structures, supported with the rough surface morphology in Fig. 4(a). This concentration depth profile supports the notion that the W concentration is indeed modulated and should be related with the exceptionally slow MIT character of our W-VO<sub>2</sub> films.

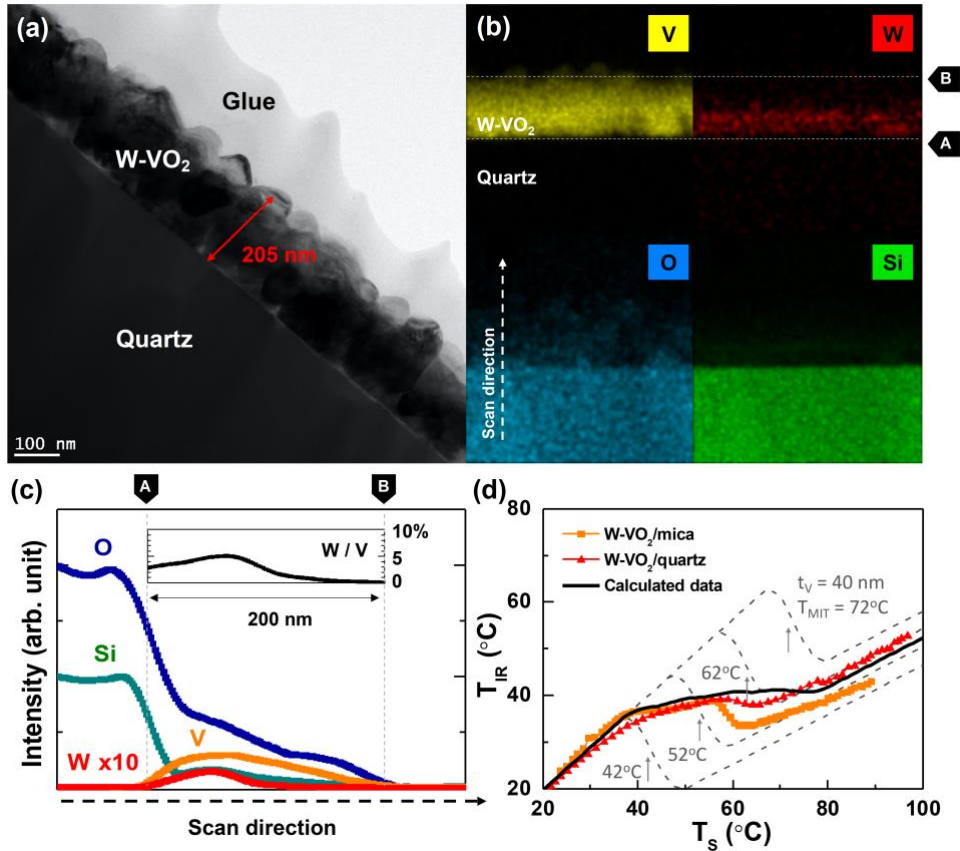


Figure 4. Microscopic analysis of the W-VO<sub>2</sub> film. (a) Cross-section TEM image, (b) energy dispersive spectroscopy mapping of four elements (V, W, O, and Si), and (c) elemental depth profiles of a W-VO<sub>2</sub> film ( $t_v = 96$  nm) on a quartz substrate. (d) Calculation of  $T_{IR}$  versus  $T_s$  curve for the W-VO<sub>2</sub> film. We duplicated and shifted the temperature measured by IR camera ( $T_{IR}$ ) of  $t_v = 40$  nm sample with 10°C decrement of transition temperature. By averaging the shifted curves, we could fit the experimental curves with the calculated one.

To understand the relation between the modulated concentration profile and the thermal stealth effect, we attempted to calculate the  $T_{IR}$ - $T_s$  curves of the W-VO<sub>2</sub> films with simple assumptions. Previous studies on W-VO<sub>2</sub> films have revealed that a homogeneous W doping weakens the MIT characteristics of VO<sub>2</sub> films and lowers the  $T_{MIT}$  of pure VO<sub>2</sub> films in a concentration dependent manner[42,43]. Based on this and the concentration depth profile in Fig. 4(c), we

calculated a  $T_{IR}$  versus  $T_S$  curve for the W-VO<sub>2</sub> films with W dopant concentration gradient. First, we choose the  $T_{IR}$  versus  $T_S$  data of a VO<sub>2</sub> film ( $t_V = 40$  nm) as a reference layer. For simplicity, we assume a stack of four W-VO<sub>2</sub> layers with four different tungsten dopant concentration and  $T_{MIT}$  values (= 72, 62, 52, and 42°C). Those W-VO<sub>2</sub> layers are expected to give four  $T_{IR}$  versus  $T_S$  curves with shifted  $T_{MIT}$  values, shown as four dashed gray curves in Fig. 4(d), respectively. By calculating the average of those four different  $T_{IR}$  versus  $T_S$  curves, we generated a  $T_{IR}$  versus  $T_S$  curve (a black curve in Fig. 4(d)), which follows the experimental curve for both the W-VO<sub>2</sub> films on quartz (a red one) and mica (a pink one). The similarity between the calculated and experimental curves demonstrates that the thermal stealth behavior improved in W-VO<sub>2</sub> films might stem from the inhomogeneous W concentration in the films.

Finally, we demonstrated a remarkable improvement of the thermal stealth properties from W-doping-induced attenuation of MIT in VO<sub>2</sub> films. On a flexible mica substrate, we also showed the thermal stealth behavior similar to that on the quartz, brightening application of the films highly feasible to curved surfaces. Combined with passive operation without external electrical power, we believe that our findings may provide a low cost and low energy method for a practical application of MIT materials to the military stealth equipment, and passive smart window devices[44,45]. We also showed that such an improvement in the passive thermal stealth characteristics is reproduced also in a stack of VO<sub>2</sub> layers with a control of spatial W concentration. Similar improvement of thermal stealth capability has been observed in multilayered thin films[46,47]. In addition, tuning the temperature coefficient of resistance of W-VO<sub>2</sub> films may improve the IR sensing performance of the bolometer, a key component for IR-temperature and -image sensors[48].

## IV. CONCLUSION

We fabricated VO<sub>2</sub> and W-VO<sub>2</sub> thin films by e-beam evaporation with subsequent oxidation and studied the thermal stealth effects of these films by investigating their IR emission properties. The W-VO<sub>2</sub> films exhibited the thermal stealth effects at lower temperatures and over a wider range of temperature than the VO<sub>2</sub> films, and the microscopic chemical composition analysis revealed that the tungsten dopant was gradually distributed toward the substrate/film interface during the thermal oxidation process. We conclude that the enhanced thermal stealth effects of the W-VO<sub>2</sub> films are primarily due to the W gradient doping. Our results suggest a unique solution to overcome the drawbacks of VO<sub>2</sub> film stemming from its sharp MIT and large hysteresis characteristics, which may bring the applications of MIT materials to the fields, such as passive thermal camouflage, flexible smart windows, and improved IR sensors, forward.

## Acknowledgements

This work is supported by the National Research Foundation of Korea (NRF) grants funded by the Korea government (NRF-2020R1A2C200373211). This research was supported by Nano·Material Technology Development Program through the National Research Foundation of Korea (NRF) funded by the Ministry of Science, ICT and Future Planning, Korea (2009-0082580). S.-H. Phark acknowledges support from IBS-R027-D1.

## References

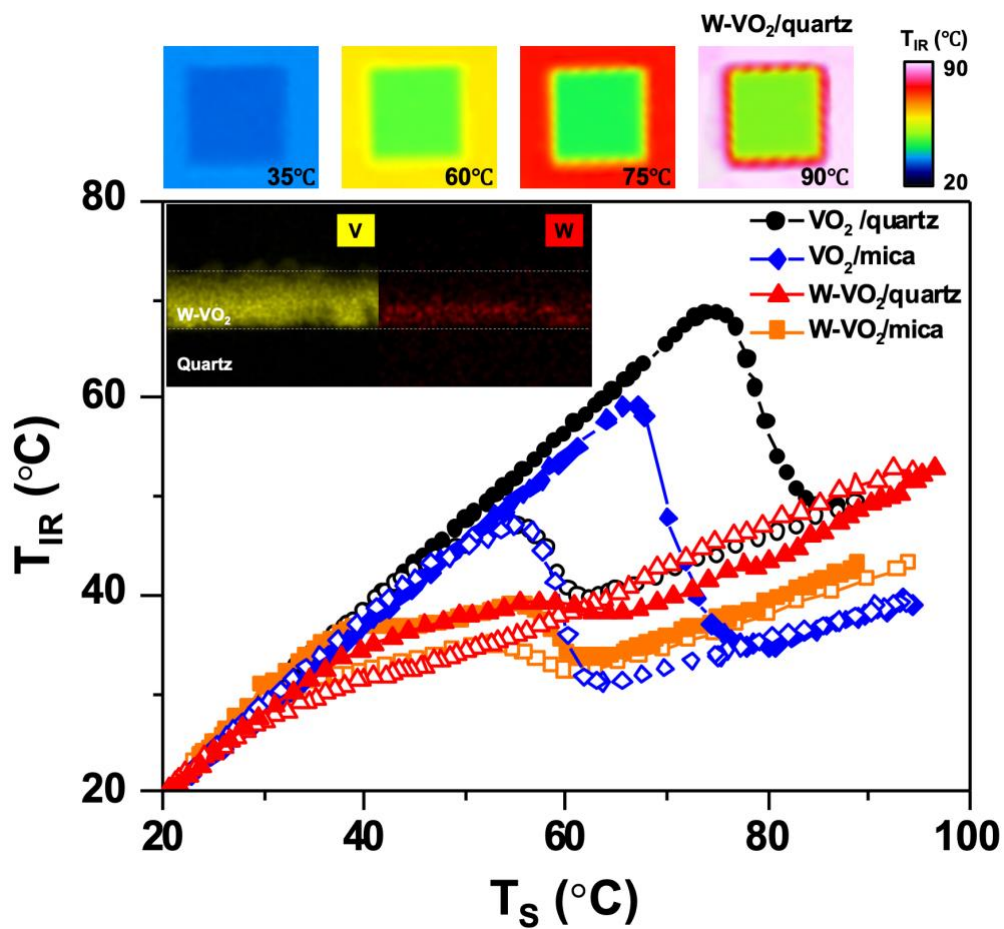
- [1] M.A. Kats, R. Blanchard, S. Zhang, P. Genevet, C. Ko, S. Ramanathan, F. Capasso, Vanadium dioxide as a natural disordered metamaterial: Perfect thermal emission and large broadband negative differential thermal emittance, *Phys. Rev. X.* 3 (2014) 1–7. <https://doi.org/10.1103/PhysRevX.3.041004>.
- [2] L. Xiao, H. Ma, J. Liu, W. Zhao, Y. Jia, Q. Zhao, K. Liu, Y. Wu, Y. Wei, S. Fan, K. Jiang, Fast Adaptive Thermal Camouflage Based on Flexible VO<sub>2</sub>/Graphene/CNT Thin Films, *Nano Lett.* 15 (2015) 8365–8370. <https://doi.org/10.1021/acs.nanolett.5b04090>.
- [3] O. Salihoglu, H.B. Uzlu, O. Yakar, S. Aas, O. Balci, N. Kakenov, S. Balci, S. Olcum, S. Süzer, C. Kocabas, Graphene-Based Adaptive Thermal Camouflage, *Nano Lett.* 18 (2018) 4541–4548. <https://doi.org/10.1021/acs.nanolett.8b01746>.
- [4] E.M. Leung, M. Colorado Escobar, G.T. Stiubianu, S.R. Jim, A.L. Vyatskikh, Z. Feng, N. Garner, P. Patel, K.L. Naughton, M. Follador, E. Karshalev, M.D. Trexler, A.A. Gorodetsky, A dynamic thermoregulatory material inspired by squid skin, *Nat. Commun.* 10 (2019) 1947. <https://doi.org/10.1038/s41467-019-09589-w>.
- [5] H. Demiryont, D. Moorehead, Electrochromic emissivity modulator for spacecraft thermal management, *Sol. Energy Mater. Sol. Cells.* 93 (2009) 2075–2078. <https://doi.org/10.1016/j.solmat.2009.02.025>.
- [6] H. Li, K. Xie, Y. Pan, M. Yao, C. Xin, Variable emissivity infrared electrochromic device based on polyaniline conducting polymer, *Synth. Met.* 159 (2009) 1386–1388. <https://doi.org/10.1016/j.synthmet.2009.02.028>.
- [7] B. Kim, J.K. Koh, J. Park, C. Ahn, J. Ahn, J.H. Kim, S. Jeon, Patternable PEDOT nanofilms with grid electrodes for transparent electrochromic devices targeting thermal camouflage, *Nano Converg.* 2 (2015) 19. <https://doi.org/10.1186/s40580-015-0051-9>.
- [8] T. Inoue, M. De Zoysa, T. Asano, S. Noda, Realization of narrowband thermal emission with optical nanostructures, *Optica.* 2 (2015) 27. <https://doi.org/10.1364/OPTICA.2.000027>.
- [9] H. Kim, Y. Kim, T. Kim, A.-R. Jang, H.Y. Jeong, S.H. Han, D.H. Yoon, H.S. Shin, D.J. Bae, K.S. Kim, W.S. Yang, Enhanced optical response of hybridized VO<sub>2</sub>/graphene films, *Nanoscale.* 5 (2013) 2632–2636. <https://doi.org/10.1039/C3NR34054F>.
- [10] K. Ito, T. Matsui, H. Iizuka, Thermal emission control by evanescent wave coupling between guided mode of resonant grating and surface phonon polariton on silicon carbide plate, *Appl. Phys. Lett.* 104 (2014) 1–6. <https://doi.org/10.1063/1.4864401>.
- [11] Z. Wang, J.K. Clark, L.C. Huang, Y.L. Ho, J.J. Delaunay, Plasmonic nanochannel structure for narrow-band selective thermal emitter, *Appl. Phys. Lett.* 110 (2017) 251102. <https://doi.org/10.1063/1.4989692>.
- [12] R. Shi, N. Shen, J. Wang, W. Wang, A. Amini, N. Wang, C. Cheng, Recent advances in fabrication strategies, phase transition modulation, and advanced applications of vanadium dioxide, *Appl. Phys. Rev.* 6 (2019) 11312. <https://doi.org/10.1063/1.5087864>.

- [13] C. Zhang, C. Koughia, Y. Li, X. Cui, F. Ye, S. Shiri, M. Sanayei, S.-J. Wen, Q. Yang, S. Kasap, Near-zero IR transmission of VO<sub>2</sub> thin films deposited on Si substrate, *Appl. Surf. Sci.* 440 (2018) 415–420. <https://doi.org/10.1016/J.APSUSC.2018.01.176>.
- [14] Y. Shimakawa, T. Yoshitake, Y. Kubo, T. Machida, K. Shinagawa, A. Okamoto, Y. Nakamura, A. Ochi, S. Tachikawa, A. Ohnishi, A variable-emittance radiator based on a metal–insulator transition of (La,Sr)MnO<sub>3</sub> thin films, *Appl. Phys. Lett.* 80 (2002) 4864–4866. <https://doi.org/10.1063/1.1489079>.
- [15] A. Shahsafi, P. Roney, Y. Zhou, Z. Zhang, Y. Xiao, C. Wan, R. Wambold, J. Salman, Z. Yu, J. Li, J.T. Sadowski, R. Comin, S. Ramanathan, M.A. Kats, Temperature-independent thermal radiation, *Proc. Natl. Acad. Sci.* 116 (2019) 26402–26406. <https://doi.org/10.1073/PNAS.1911244116>.
- [16] Y. Shimakawa, T. Yoshitake, Y. Kubo, T. Machida, K. Shinagawa, A. Okamoto, Y. Nakamura, A. Ochi, S. Tachikawa, A. Ohnishi, A variable-emittance radiator based on a metal–insulator transition of (La,Sr)MnO<sub>3</sub> thin films, *Appl. Phys. Lett.* 80 (2002) 4864–4866. <https://doi.org/10.1063/1.1489079>.
- [17] M. Kamalisarvestani, R. Saidur, S. Mekhilef, F.S. Javadi, Performance, materials and coating technologies of thermochromic thin films on smart windows, *Renew. Sustain. Energy Rev.* 26 (2013) 353–364. <https://doi.org/10.1016/J.RSER.2013.05.038>.
- [18] X. Cao, P. Jin, Solar Modulation Utilizing VO<sub>2</sub>-Based Thermochromic Coatings for Energy-Saving Applications, *Emerg. Sol. Energy Mater.* (2018) 1.
- [19] F.P. Lang, H. Wang, S.J. Zhang, J.B. Liu, H. Yan, Review on Variable Emissivity Materials and Devices Based on Smart Chromism, *Int. J. Thermophys.* 39 (2018) 1–20. <https://doi.org/10.1007/s10765-017-2329-0>.
- [20] B. Yoshichika, N. Koichi, K. Yasutoshi, T. Toshio, Growth of VO<sub>2</sub> Single Crystals by Chemical Transport Reaction, *Jpn. J. Appl. Phys.* 8 (1969) 633.
- [21] H. Jerominek, F. Picard, N.R. Swart, M. Renaud, M. Levesque, M. Lehoux, J.-S. Castonguay, M. Pelletier, G. Bilodeau, D. Audet, T.D. Pope, P. Lambert, Micromachined uncooled VO<sub>2</sub>-based IR bolometer arrays, in: *Proc.SPIE*, 1996. <https://doi.org/10.1117/12.243056>.
- [22] G. Rampelberg, B. De Schutter, W. Devulder, K. Martens, I. Radu, C. Detavernier, In situ X-ray diffraction study of the controlled oxidation and reduction in the V–O system for the synthesis of VO<sub>2</sub> and V<sub>2</sub>O<sub>3</sub> thin films, *J. Mater. Chem. C.* 3 (2015) 11357–11365. <https://doi.org/10.1039/C5TC02553B>.
- [23] H. Paik, J.A. Moyer, T. Spila, J.W. Tashman, J.A. Mundy, E. Freeman, N. Shukla, J.M. Lapano, R. Engel-Herbert, W. Zander, J. Schubert, D.A. Muller, S. Datta, P. Schiffer, D.G. Schlom, Transport properties of ultra-thin VO<sub>2</sub> films on (001) TiO<sub>2</sub> grown by reactive molecular-beam epitaxy, *Appl. Phys. Lett.* 107 (2015) 3–8. <https://doi.org/10.1063/1.4932123>.
- [24] X. Tan, T. Yao, R. Long, Z. Sun, Y. Feng, H. Cheng, X. Yuan, W. Zhang, Q. Liu, C. Wu, Y. Xie, S. Wei, Unraveling metal-insulator transition mechanism of VO<sub>2</sub> triggered by tungsten doping, *Sci. Rep.* 2 (2012) 1–6. <https://doi.org/10.1038/srep00466>.
- [25] K. Shibuya, M. Kawasaki, Y. Tokura, Metal-insulator transition in epitaxial

- V<sub>1-x</sub>W<sub>x</sub>O<sub>2</sub> (0 ≤ x ≤ 0.33) thin films, *Appl. Phys. Lett.* 96 (2010) 22102.  
<https://doi.org/10.1063/1.3291053>.
- [26] H. Takami, T. Kanki, S. Ueda, K. Kobayashi, H. Tanaka, Filling-controlled Mott transition in W-doped VO<sub>2</sub>, *Phys. Rev. B.* 85 (2012) 205111.  
<https://doi.org/10.1103/PhysRevB.85.205111>.
- [27] D. Liu, H. Cheng, X. Xing, C. Zhang, W. Zheng, Thermochromic properties of W-doped VO<sub>2</sub> thin films deposited by aqueous sol-gel method for adaptive infrared stealth application, *Infrared Phys. Technol.* 77 (2016) 339–343.  
<https://doi.org/10.1016/j.infrared.2016.06.019>.
- [28] T.J. Hanlon, J.A. Coath, M.A. Richardson, Molybdenum-doped vanadium dioxide coatings on glass produced by the aqueous sol-gel method, *Thin Solid Films.* 436 (2003) 269–272. [https://doi.org/10.1016/S0040-6090\(03\)00602-3](https://doi.org/10.1016/S0040-6090(03)00602-3).
- [29] D.A. Vinichenko, V.P. Zlomanov, V.A. Vasil'ev, D.S. Seregin, O.Y. Berezina, Synthesis of vanadium dioxide films by a modified sol-gel process, *Inorg. Mater.* 47 (2011) 279–284. <https://doi.org/10.1134/S0020168511030216>.
- [30] S. Kumar, F. Maury, N. Bahlawane, Electrical Switching in Semiconductor-Metal Self-Assembled VO<sub>2</sub> Disordered Metamaterial Coatings, *Sci. Rep.* 6 (2016) 1–13.  
<https://doi.org/10.1038/srep37699>.
- [31] Y.J. Chang, C.H. Koo, J.S. Yang, Y.S. Kim, D.H. Kim, J.S. Lee, T.W. Noh, H.-T. Kim, B.G. Chae, Phase coexistence in the metal–insulator transition of a VO<sub>2</sub> thin film, *Thin Solid Films.* 486 (2005) 46–49. <https://doi.org/10.1016/J.TSF.2004.11.220>.
- [32] S. Lee, T.L. Meyer, S. Park, T. Egami, H.N. Lee, Growth control of the oxidation state in vanadium oxide thin films, *Appl. Phys. Lett.* 105 (2014) 223515.  
<https://doi.org/10.1063/1.4903348>.
- [33] X. Lv, Y. Cao, L. Yan, Y. Li, L. Song, Atomic layer deposition of VO<sub>2</sub> films with Tetrakis-dimethyl-amino vanadium (IV) as vanadium precursor, *Appl. Surf. Sci.* 396 (2017) 214–220. <https://doi.org/10.1016/J.APSUSC.2016.10.044>.
- [34] S.J. Yun, J.W. Lim, J.S. Noh, B.G. Chae, H.T. Kim, Vanadium dioxide films deposited on amorphous SiO<sub>2</sub> - And Al<sub>2</sub> O<sub>3</sub> -coated Si substrates by reactive RF-magnetron sputter deposition, *Jpn. J. Appl. Phys.* 47 (2008) 3067–3069.  
<https://doi.org/10.1143/JJAP.47.3067>.
- [35] X. Liu, S.-W. Wang, F. Chen, L. Yu, X. Chen, Tuning phase transition temperature of VO<sub>2</sub> thin films by annealing atmosphere, *J. Phys. D. Appl. Phys.* 48 (2015) 265104.  
<https://doi.org/10.1088/0022-3727/48/26/265104>.
- [36] A. Rogalski, *Infrared detectors*, CRC press, 2010.
- [37] A.S. Oleinik, Optical Data Recording with Vanadium Dioxide – Based Film Reversible Media, *Tech. Phys.* 47 (2002) 1014–1018.
- [38] S.J. Jiang, C.B. Ye, M.S.R. Khan, C.-G. Granqvist, Evolution of thermochromism during oxidation of evaporated vanadium films, *Appl. Opt.* 30 (1991) 847–851.  
<https://doi.org/10.1364/AO.30.000847>.
- [39] J. Crank, *The mathematics of diffusion* 2nd Edition, Oxford Sci. Publ. (1975) 32.

- [40] Z. Luo, Z. Wu, X. Xu, M. Du, T. Wang, Y. Jiang, Microstructures and thermochromic properties of tungsten doped vanadium oxide film prepared by using  $\text{VO}_x\text{-W-VO}_x$  sandwich structure, *Mater. Sci. Eng. B.* 176 (2011) 762–766.  
<https://doi.org/10.1016/J.MSEB.2011.02.022>.
- [41] R.J.D. Tilley, *Defects in solids*, John Wiley & Sons, 2008.
- [42] A. Romanyuk, R. Steiner, L. Marot, P. Oelhafen, Temperature-induced metal-semiconductor transition in W-doped  $\text{VO}_2$  films studied by photoelectron spectroscopy, *Sol. Energy Mater. Sol. Cells.* 91 (2007) 1831–1835.  
<https://doi.org/10.1016/j.solmat.2007.06.013>.
- [43] S.E. Chen, H.H. Lu, S. Brahma, J.L. Huang, Effects of annealing on thermochromic properties of W-doped vanadium dioxide thin films deposited by electron beam evaporation, *Thin Solid Films.* 644 (2017) 52–56.  
<https://doi.org/10.1016/j.tsf.2017.05.052>.
- [44] Y. Kim, S. Yu, J. Park, D. Yoon, A.M. Dayaghi, K.J. Kim, J.S. Ahn, J. Son, High-throughput roll-to-roll fabrication of flexible thermochromic coatings for smart windows with  $\text{VO}_2$  nanoparticles, *J. Mater. Chem. C.* 6 (2018) 3451–3458.  
<https://doi.org/10.1039/c7tc05876d>.
- [45] H. Kim, Y. Kim, K.S. Kim, H.Y. Jeong, A.-R. Jang, S.H. Han, D.H. Yoon, K.S. Suh, H.S. Shin, T. Kim, W.S. Yang, Flexible Thermochromic Window Based on Hybridized  $\text{VO}_2$  /Graphene, *ACS Nano.* 7 (2013) 5769–5776.  
<https://doi.org/10.1021/nn400358x>.
- [46] L. Peng, D. Liu, H. Cheng, S. Zhou, M. Zu, A Multilayer Film Based Selective Thermal Emitter for Infrared Stealth Technology, *Adv. Opt. Mater.* 6 (2018) 1801006.  
<https://doi.org/10.1002/adom.201801006>.
- [47] X. Wang, Y. Cao, Y. Zhang, L. Yan, Y. Li, Fabrication of  $\text{VO}_2$  -based multilayer structure with variable emittance, *Appl. Surf. Sci.* 344 (2015) 230–235.  
<https://doi.org/10.1016/J.APSUSC.2015.03.116>.
- [48] H. Takami, K. Kawatani, T. Kanki, H. Tanaka, High Temperature-Coefficient of Resistance at Room Temperature in W-Doped  $\text{VO}_2$  Thin Films on  $\text{Al}_2\text{O}_3$  Substrate and Their Thickness Dependence, *Jpn. J. Appl. Phys.* 50 (2011) 55804.  
<https://doi.org/10.1143/jjap.50.055804>.

## Graphic Abstract



Enhanced passive thermal stealth properties in W-doped  $VO_2$  thin films, whose infrared temperature ( $T_{IR}$ ) maintains over wider substrate temperature ( $T_S$ ) range than pure  $VO_2$  thin films.